JACS
JOURNAL OF THE AMERICAN CHEMICAL SOCIETY

ARTICLE

pubs.acs.org/JACS

Continuous Transition from 3D to 1D Confinement Observed during the Formation of CdSe Nanoplatelets

S. Ithurria,[†] G. Bousquet,[†,‡] and B. Dubertret*[,†]

[†]Laboratoire de Physique et d'Etude des Matériaux, UMR8213 CNRS, ESPCI, 10 rue Vauquelin, 75231 Paris Cedex 5, France

[‡]Ecole Normale Supérieure, 45 rue d'Ulm, 75005 Paris, France

Supporting Information

ABSTRACT: We study the formation of colloidal CdSe nanoplatelets using both tansmission electron microscopy (TEM) and spectroscopic analysis. We show that the platelets form by continuous lateral extension of small (<2 nm) nanocrystal CdSe seeds. The nanoplatelet thickness is fixed by the seed dimension and remains constant during the platelet formation. The nanoplatelet lateral dimensions can be tuned using additional precursor injection. Absorption and fluorescence analysis of the CdSe nanoplatelets as they continuously extend laterally confirms a continuous transition from 3D to 1D confined nanoparticles. The formation of the CdSe platelets is found to be similar for different platelet thicknesses that we control with a precision of one CdSe monolayer.

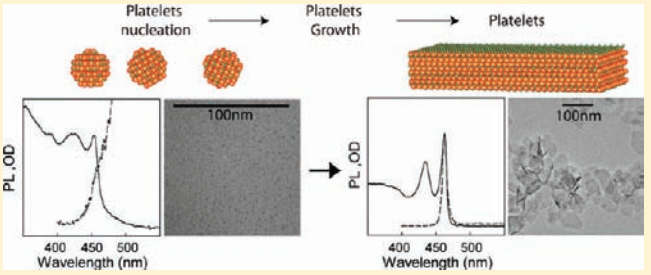

Two-dimensional colloidal anisotropic inorganic crystal nanostructures, especially those with thickness < 10 nm, have recently emerged as a novel class of material with unusual electronic and optical properties resulting from their exceptionally small thickness and their lateral dimensions that can reach several micrometers. In the past few years, the number of ultrathin 2D nanosheets synthesized has grown rapidly. Examples of materials include metals (Ag,[1] Au,[2] Co[3]), metal oxides,[4,5] rare-earth oxides,[6,7] and semiconductors.[8,9] Most of the work published so far focuses primarily on the growth mechanisms and the structural characterization of these 2D ultrathin films crystals. Several formation mechanisms have been reported. They include oriented attachment,[10] self-organization of initially formed small nanocrystals followed by an in situ recrystallization process,[11,12] and soft template methods.[13]

One type of 2D materials of particular interest are the semiconductors because their optical properties should be similar to those of quantum wells. Semiconductor nanocrystals have been synthesized with various shapes including spheres,[14] rods,[15] tetrapods,[16] and, recently, platelets.[17] While optical spectroscopy of quantum dots and nanorods is a good technique to characterize their electronic structures,[18] their shape, their monodispersity,[14] their surface chemistry,[19] and their crystal structures,[20] such a technique has been used in the case of semiconductor nanoplatelets only in a few examples.[9,17]

In this work, we study the formation of cubic CdSe nanoplatelets (NPLs). Hexagonal CdSe nanoribbons have been shown to form through soft template molding,[13] but the formation mechanism of 2D zinc blende free-standing CdSe NPLs that have no intrinsic driving force for 2D anisotropic growth is still not understood. We explore the formation mechanisms of these CdSe NPLs using a combination of transmission electron microscopy (TEM) images and absorption and emission spectra. We show that the NPLs growth starts with the formation of ∼2 nm diameter seeds that subsequently extend laterally to form NPLs. The NPLs thickness is constant during the growth and is fixed by the seed dimension. Fluorescence and absorption analysis during the NPLs formation is consistent with a continuous transition from a 3D to a 1D confined nanoparticle. Detailed analysis of the transition provides information on the NPLs lateral dimensions and confirms the 1D confinement already observed in these systems.

EXPERIMENTAL SECTION

Cadmium nitrate dihydrate, cadmium acetate tetrahydrate, trioctylphosphine (TOP), technical grade 1-octadecene (ODE), myristic acid sodium salt, and selenium in powder were purchased from Sigma Aldrich. Methanol, ethanol, and hexane were purchased from SDS Carlo Erba.

Precursor Preparation. Preparation of Cd(myristate)$_2$: 1.23 g of Cd(nitrate)$_2$ is dissolved in 40 mL of methanol, 3.13 g of Na(myristate) is dissolved in 250 mL of methanol. These two solutions are mixed, and the resulting precipitate of Cd(myristate)$_2$ is filtered, is rinsed several times with methanol, and is dried under vacuum overnight.

Preparation of TOPSe at 1 M: In a glovebox, 395 mg (0.05 mol) of selenium is dissolved by agitation in a flask with 50 mL of TOP.

Preparation of SeODE at 0.1 M: 70 mL of octadecene is introduced in a three-neck flask. Under argon flow, the mixture is heated at 180 °C. Seventy-nine milligrams (0.01 mol) of selenium mesh is sonicated into 30 mL of

Received: November 9, 2010
Published: February 16, 2011

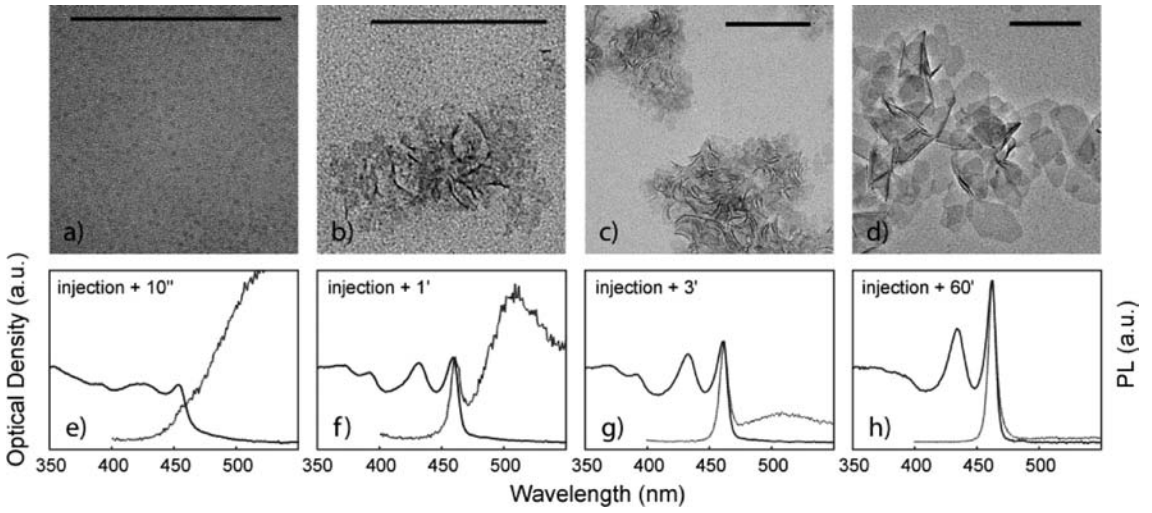

Figure 1. Growth stages of CdSe nano platelets. Top: Transmission electron microscope images of the CdSe particles 10 s (a), 60 s (b), 180 s (c), and 1 h (d) after the injection of TOPSe. Samples are deposited directly in the TEM grid without washing. Scale bars: 100 nm. Bottom: corresponding absorption (plain line) and emission spectra (dotted lines) of the samples.

octadecene and is slowly introduced into the three-neck flask. Once the selenium is totally introduced, the mixture is heated at 220 °C for 30 min.

Protocol 1: Nanoplatelets Emitting at 460 nm. In a three-neck flask, 240 mg of $Cd(Ac)_2$, 286 μL of oleic acid, and 15 mL of octadecene are degassed under vacuum flow for 1 h at 80 °C. The mixture is then heated at 170 °C under argon flow, and a syringe of 150 μL of TOPSe at 1 M is injected. The reaction is total after 45 minutes.

Protocol 2: Slow Formation of 460 nm and 510 nm Emitting Nanoplatelet Populations. In a three-neck flask, 170 mg of $Cd(myr)_2$, 12 mg of Se, and 15 mL of octadecene are degassed under vacuum for 1 h. The mixture is heated at 134 °C for 290 min under argon flow, and then 55 mg of $Zn(Ac)_2$ is introduced. The mixture is then slowly heated to 230 °C. After a total reaction time of 450 min (7 h 30 min), the solution is brought to room temperature with an injection of 1 mL of oleic acid. The mixture of NPLs and quantum dots (QDs) is suspended in hexane after a precipitation in ethanol.

Nanoplatelets Emitting at 512 nm. In a three-neck flask, 170 mg of $Cd(myr)_2$, 12 mg of Se, and 15 mL of octadecene are degassed under vacuum for 1 h. The mixture is heated at 240 °C under argon flow; when the temperature mixture has reached 190 °C, 55 mg of $Zn(Ac)_2$ is introduced. After heating for 5 min at 240 °C, the solution is rapidly brought to room temperature. At room temperature, 1 mL of oleic acid is added to the mixture with hexane. The NPLs are separated from the QDs using centrifugation at 5000 rpm. The QDs remain suspended in the supernatant, whereas the NPLs precipitate. The supernatant is discarded, and the NPLs are suspended in hexane.

Nanoplatelets Emitting at 550 nm. In a three-neck flask, 170 mg of $Cd(myr)_2$, 12 mg of Se, and 15 mL of octadecene are degassed under vacuum for 1 h. The mixture is heated at 240 °C under argon flow; when the temperature mixture has reached 190 °C, 160 mg of $Cd(Ac)_2$ is introduced. After 10 min at 240 °C, 1.5 mL of SeODE at 0.1 M is injected. After 5 min at 240 °C, the reaction is stopped. At room temperature, 1 mL of oleic acid is added to the mixture with hexane. The NPLs are separated from the QDs using centrifugation at 5000 rpm. The NPLs emitting at 550 nm are less soluble than those emitting at 513 nm and can be isolated using successive precipitations.

RESULTS AND DISCUSSION

Nanoplatelet Formation Monitored Using TEM and Absorption/Emission Spectra. We first analyzed 460 nm emitting NPLs synthesized using protocol 1. This synthesis is based on the injection of precursors in a hot solution. It is rapid and produces NPLs with one thickness only. No other type of nanoparticles, like regular quantum dots, could be detected at the end of this synthesis. Samples of the reaction mixture were taken 10 s, 60 s, 3 min, and 1 h after the beginning of the reaction and were analyzed without further processing (not even sonication) using both transmission electron microscopy (TEM) and spectroscopic analysis (Figure 1).

Ten seconds after the onset of the reaction, small CdSe nanoparticles that are around 2 nm diameter are visible on the TEM images (Figure 1a). The absorption spectrum of the reaction mixtures at this stage displays well-defined features (Figure 1e) and is typical of CdSe 2 nm diameter nanoparticles obtained by another method.[21] The first absorption maximum, which corresponds to the first excitonic absorption, is located at 455 nm as expected for 2 nm diameter CdSe nanoparticles.[22] The sample emission spectrum (Figure 1e) only shows broad fluorescence, characteristics of deep trap fluorescence, often observed in very small CdSe clusters.[23]

Sixty seconds after the beginning of the reaction, a few nanometers wide CdSe NPLs are seen on TEM images (Figure 1b), while some 2 nm diameter CdSe nanoparticles remain visible. The small NPLs are mostly aggregated to each other. We observe a 4 nm red shift of the sample's first exciton absorption (Figure 1f) at 459 nm, which suggests particle growth. A second, well-defined, absorption maximum with similar strength appears at 432 nm. The emission spectra (Figure 1f) display a mixture of deep trap and band edge fluorescence. Interestingly, the band edge fluorescence is 14 nm full width at half-maximum (fwhm), and the Stokes shift is 2 nm. These two values are much smaller compared to usual CdSe polyhedric nanoparticles.[21]

Three minutes after the precursor injection, larger aggregates of NPLs with larger lateral dimensions (a few tens of nanometers) are visible on TEM images (Figure 1c). The three main features of the absorption spectrum present at 60 s are still present, shifted to longer wavelengths by a few nanometers (Figure 1g). The fluorescence deep trap emission has substantially decreased, and the fluorescence emission spectrum has decreased to 10 nm fwhm. The Stokes shift is less than 2 nm.

Sixty minutes after the injection, NPLs with lateral dimensions ranging from a few tens of nanometers to 100 nm are clearly visible (Figure 1h). Some of them lay flat on the TEM grid surface. Others are folded or stacked together. At this stage, 2 nm diameter nanoparticles are not visible anymore on the TEM pictures. As we pointed out recently,[17] the absorption spectrum of Figure 1h is very similar to the one of CdSe ultrathin film with the heavy hole−electron and the light hole−electron transition being assigned to the first two absorption maxima. Despite the diversity of the NPLs lateral dimensions, the emission spectrum is now 7 nm fwhm, and the Stokes shift is less than 1 nm (Figure 1h).

During the synthesis, the first exciton absorption around 460 nm (Figure 1e−h) increases continuously compared to the absorption at 350 nm. This line becomes the prominent feature of the absorption spectra in agreement with the formation and the extension of quantum wells with stable exciton at room temperature.

Single Nanoplatelet Crystal Structure and Orientation. The powder X-ray diffraction (XRD) pattern (Figure S1 of the Supporting Information) taken from the CdSe NPLs confirmed their cubic crystal structure. A high-resolution TEM (HRTEM) image taken from the top face of a single CdSe NPL revealed that the NPL contrast is extremely low even on very thin carbon film supports (Figure 2). Lattice fringes are clearly visible across the entire surface, a portion of which is magnified in Figure 2b. The whole NPL (Figure 2a) Fourier transform (FT) pattern showed an array of spots with a 4-fold rotational symmetry (Figure 2c) that can be indexed as the {220} reflections (axes zone [001]). These data indicate that the NPL is a piece of single crystal with its top and bottom faces perpendicular to the [001] direction. Moreover, the orientation of the NPLs edges are found to be perpendicular to the [100] and the [010] axis, respectively. Such crystal orientation is surprising since in a cubic structure all these axes are equivalent. It suggests a symmetry breakdown at some point during the formation of the NPLs. This symmetry breakdown could happen during the NPLs seeds formation (Figure 1a).

Low angle powder XRD (Figure S2 of the Supporting Information) showed that when NPLs are stacked together, the NPLs facets perpendicular to the [001] direction were separated by 3.75 nm, a distance close to the sum of two oleic acid chains (2 nm) and one NPL thickness (1.8 nm). The top and bottom faces of an NPL are thus in part covered with oleic acid chains.

Nanoplatelets' Seed Characterization. We did not manage to obtain precise structural data on the NPLs seeds. We observed that in a few hours, even at room temperature, and in dilute solutions, these seeds are unstable, and we did not manage to characterize them in powder XRD. TEM images reveal that their size is <2 nm (Figure 3b). They have spectroscopic features that make them different than regular nanocrystals (NCs) (Figure 3a). Their emission spectra display two features: one large peak with an important Stokes shift and an fwhm > 100 nm that is characteristic of deep trap emission and another one with no Stokes shift and an fwhm close to 10 nm that is unusual. Such small fwhm values have, to the best of our knowledge, not been reported either in regular nanocrystals or in magic size clusters.[24−26] The absorption spectra of these clusters are also different than the CdSe magic size cluster reported in previous studies.[27] Such a small fwhm suggests that at an early stage of the synthesis, we indeed have crystalline seeds that are all identical with well-defined structure and shape.

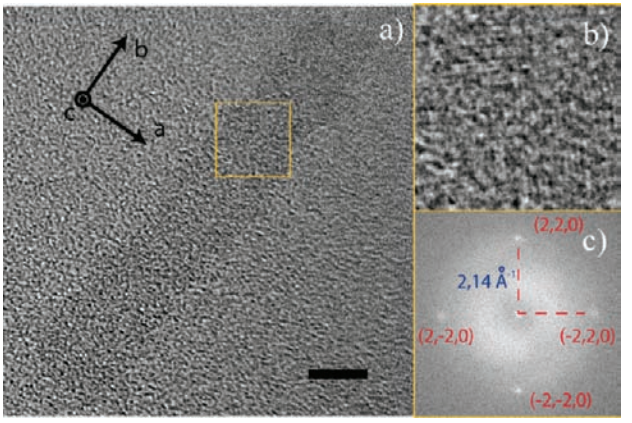

Figure 2. (a) Transmission electron microscopy image of single CdSe NPL emitting at 510 nm. The NPL is roughly 2 nm thick and spans along one diagonal of the image. The NPL main crystal axis is presented in black. Scale bar: 5 nm. (b) Magnification of part of the NPL (square shown in yellow in a) illustrating its crystallinity. (c) Fast Fourier transform (FFT) of the whole NPL demonstrating an NPL thickness parallel to the [001] direction.

Nanoplatelets' Formation Mechanisms. Figures 1a, 1e, and 3 show that the NPLs formation starts by the nucleation of nanocrystals with a diameter < 2 nm. During the synthesis, these small nanocrystals gradually disappear from the sample in TEM while NPLs with increasingly large lateral dimension appear (Figure 1b−d). The NPLs could form by self-assembly of the small seeds or by lateral extension of the seed thanks to in situ continuous reaction of Cd and Se precursors (Figure 4). Assembly of small seeds to form ultrathin 2D nanosheets has been observed during the formation of PbS ultrathin films with oriented attachment of small elementary PbS crystal seeds (path 3). In this case, the PbS NPLs obtained have a patchlike structure easily observable in TEM.[10] We did not observe such patches in any of our TEM images. On the contrary, the NPLs we observed in TEM have regular edges, and they are continuous. Another type of assembly, involving 2D self-organization of initially formed seeds followed by an in situ recrystallization process, has been observed in the case of ceria nanosheets.[11] In our case, we did not observe any recrystallization process suggesting the absence of such mechanisms for CdSe NPLs. Instead, the absorption and the emission spectra evolve smoothly during the synthesis suggesting a continuous evolution rather than a recrystallization. To further elucidate the NPLs growth process, we have analyzed the absorption spectra of fixed volume samples during the growth of the 460 nm emitting NPLs. The samples' optical density at 350 nm increases continuously from 10 s to 60 min reaction time (Figure S3 of the Supporting Information). This steady increase of the 350 nm absorption implies that CdSe in a crystalline phase is continuously forming during the synthesis. CdSe dissolution, if it takes place, is not visible in absorption. This continuous formation of CdSe in a crystalline phase can result from continuous formation of small CdSe clusters as seen in Figure 1a. These clusters would then rapidly associate to the existing NPLs to extend them laterally (Figure 4, path 1). It can also result from the NPLs extension thanks to direct precursors reaction on the NPLs edges (Figure 4, path 2).

We explored the possibility to continuously extend in solution colloidal CdSe NPLs using a slow and steady precursor injection as the NPLs form. We first synthesized 510 nm emitting NPLs.

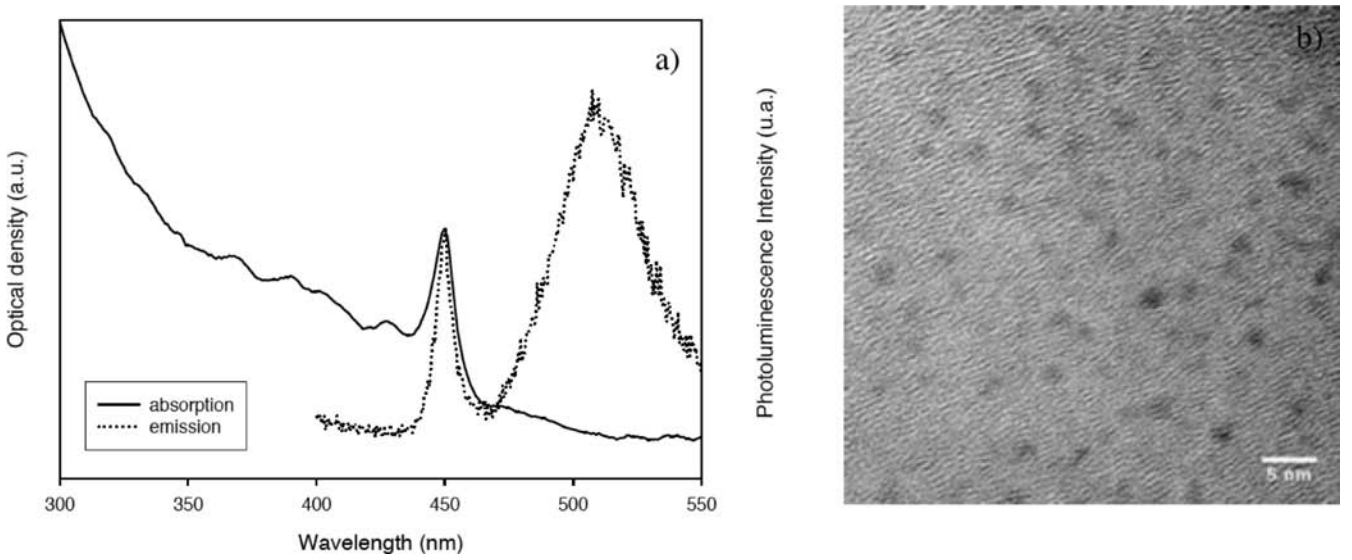

Figure 3. (a) Emission and absorption spectra of 462 nm emitting NPLs seeds and (b) TEM images of NPLs seeds precursors.

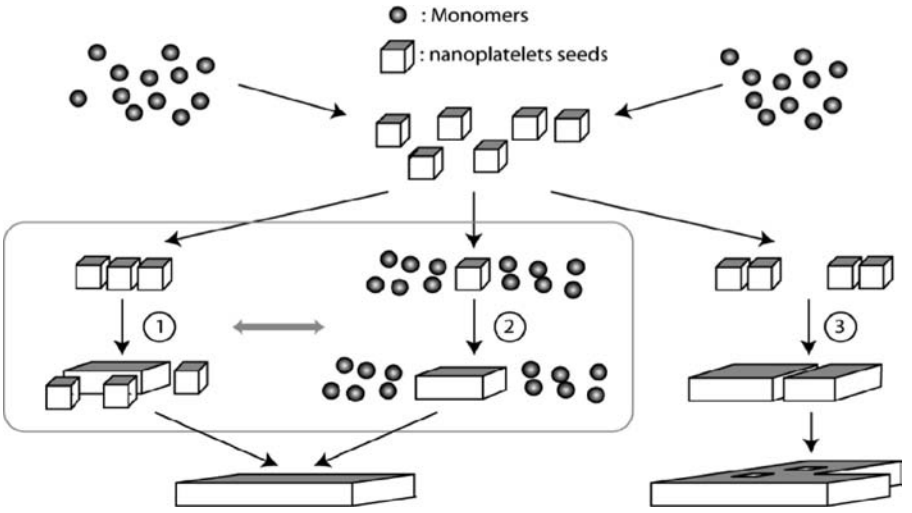

Figure 4. Possible mechanisms for the CdSe NPLs lateral extension. The first step is the formation of the NPL seeds with dimensions < 2 nm from reaction of Cd and Se precursors. In paths 1 and 3, the lateral extension results from the self-organization of seeds that assemble only at the seed level (path 1) or in patches (path 3). In path 2, the seeds form and extend laterally by continuous reaction of precursors.

We precipitated these NPLs, suspended them in hexane, and injected them in a new three-neck flask. After slow injection of Cd and Se precursors, we observed a lateral extension of the NPLs (Figure 5). Small NPL seeds cannot be detected either in TEM or in absorption/emission during the synthesis. The possibility to extend laterally the NPLs while avoiding the formation of small nanocrystals strongly suggests that the NPLs extend laterally through continuous reaction of Cd and Se precursors (Figure 4, path 2).

Continuous Transition from 3D Confined Nanocrystals to 1D Confined NPLs. We have further explored the continuous transition from 3D confined nanocrystals to 1D confined NPLs using a synthesis (see protocol 2) developed to eliminate the CdSe deep trap fluorescence even for small CdSe aggregates. This synthesis allowed us to follow continuously the fluorescence evolution of small CdSe aggregates as they transform into NPLs.

Synthesis 2 is very long: it lasts for 7 h. The temperature is slowly raised from room temperature to 230 °C, which ensures a slow and controlled growth of the colloidal nanoparticles. As opposed to the first synthesis studied above, at the end of

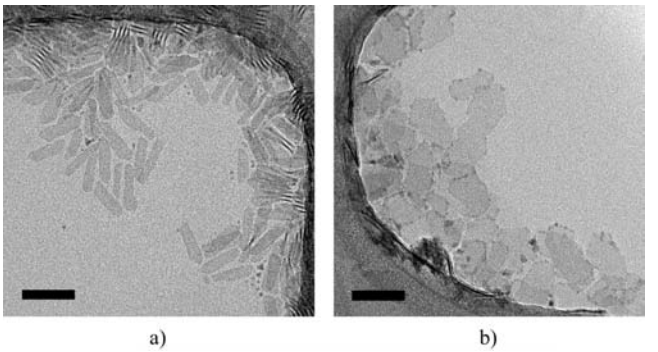

Figure 5. (a) Nanoplatelets before extension. (b) Nanoplatelets after extension with a new injection of precursors. Scale bar: 50 nm.

dx.doi.org/10.1021/ja110046d |J. Am. Chem. Soc. 2011, 133, 3070–3077

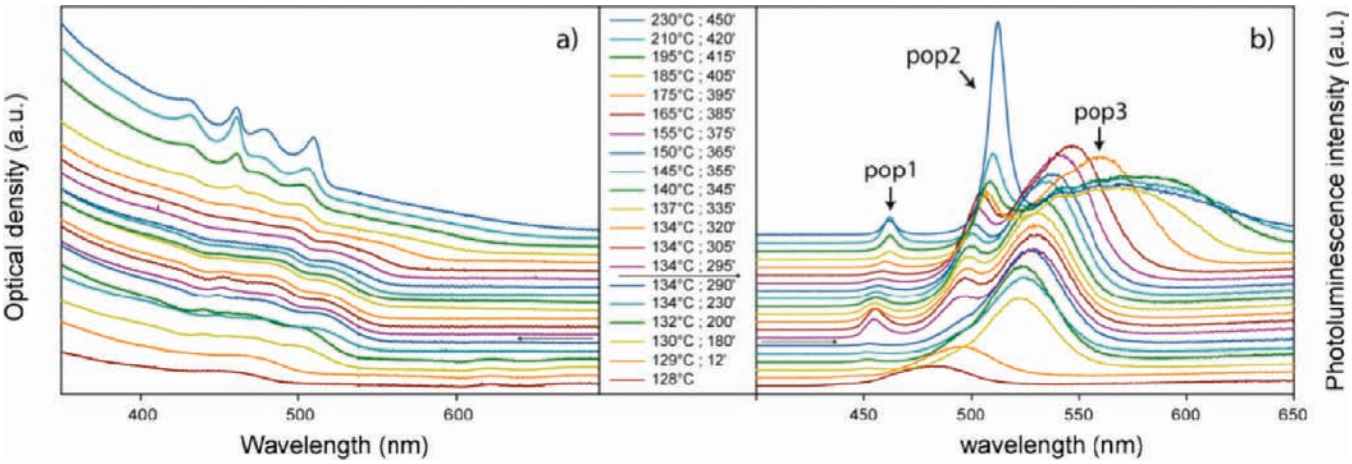

Figure 6. (a) Absorption and (b) emission spectra of CdSe nanoparticles during the growth (see Experimental Section, Protocol 2). Temperature and sampling times are indicated in the middle. Time 0 corresponds to a temperature of 128 °C. Fixed volume samples are analyzed. The arrows indicate the acetate salt injection. Three populations are clearly visible on the emission spectra.

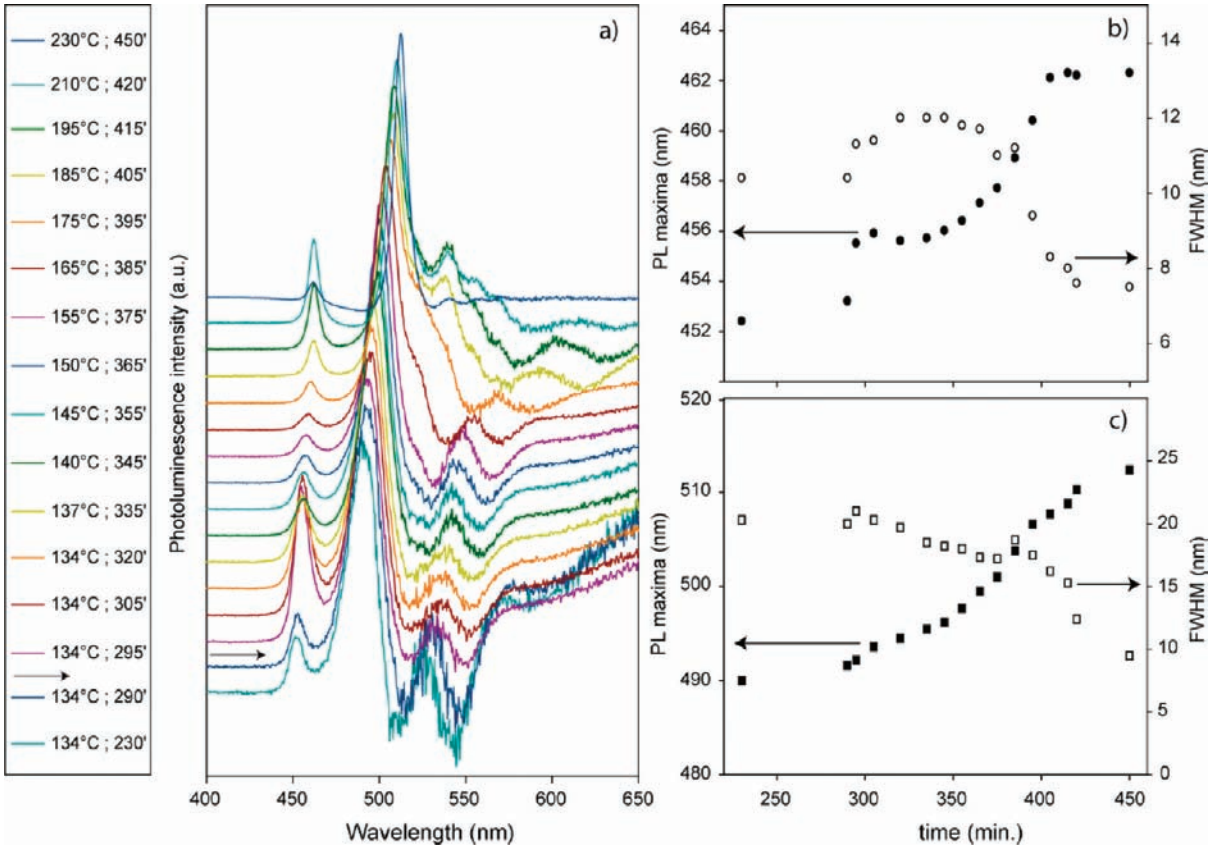

Figure 7. (a) Same spectra as in Figure 6b after subtraction for each spectrum of the gaussian emission signal corresponding to the polyhedral QDs. For clarity, each emission spectral intensity has been normalized with respect to the maximum intensity of the 510 nm population of the first sample (134C, 230′). (b) fwhm (empty circles) and emission wavelength with maximum intensity (full circles) of the NPLs emitting at 462 nm as a function of time during the synthesis. (c) fwhm (empty squares) and emission wavelength with maximum intensity (full squares) of the NPLs emitting at 513 nm as a function of time during the synthesis. Arrows in (a) indicate the acetate salt injection.

this synthesis, the reaction mixture contains two populations of NPLs with different thicknesses, named hereafter pop1 and pop2, and one population of quantum dots, pop3 (Figure 6). The absorption and emission spectra of the reaction mixture are recorded at different times during the synthesis (Figure 6). Characteristic features of each population are easily distinguishable but are tricky to analyze directly because of the cross-talk between the absorption/emission of the NCs (pop3) and the NPLs population. A possible reason for the absence of deep trap fluorescence for the NPLs could be the slow formation of the NPLs that permit a good passivation of the NPL surface traps.

dx.doi.org/10.1021/ja110046d |*J. Am. Chem. Soc.* 2011, 133, 3070–3077

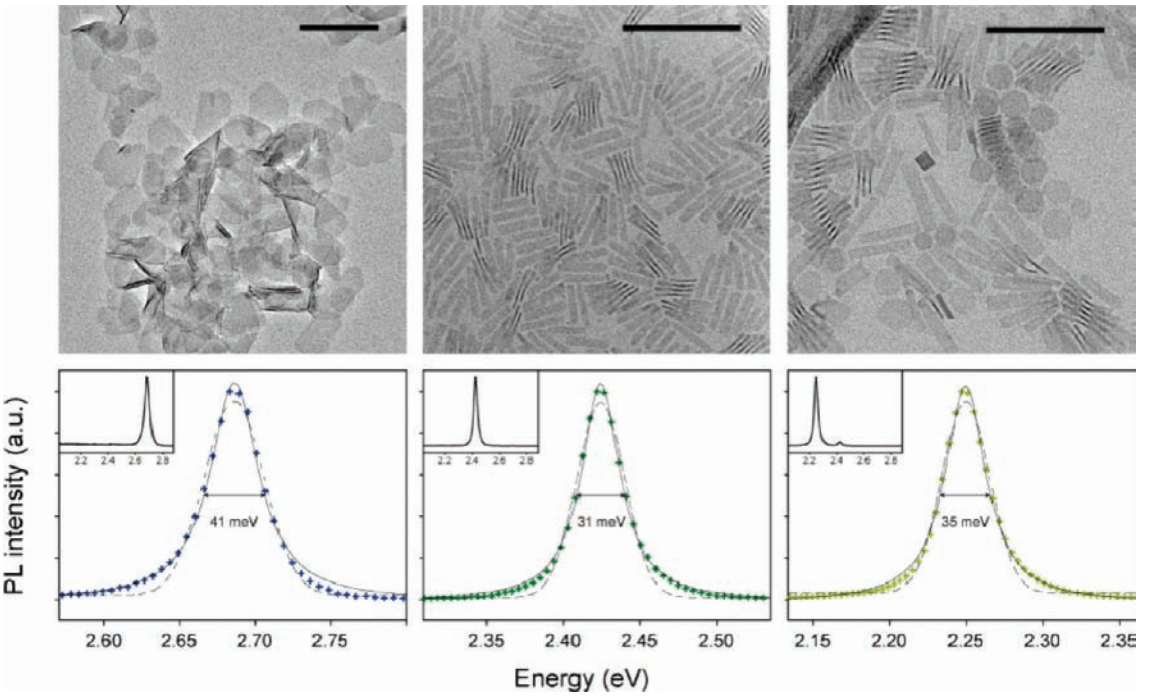

Figure 8. Top: Transmission electronic microscopy (TEM) images of three samples of NPLs emitting at wavelength 460 nm (left), 510 nm (middle), and 550 nm (right). The thickness difference between each population corresponds to one CdSe layer (3 Å). Scale bars: 100 nm. Bottom: Corresponding emission spectra (crosses) fitted with a Lorentzian (solid line) and with a Gaussian (dashed line). The insets are the emission spectra between 2.1 eV and 2.9 eV.

To minimize the cross-talk between the NPLs and the NCs emission, the emission of pop3 was fitted with a Gaussian profile, and this Gaussian was subtracted from each emission spectrum of Figure 6. This procedure gives a much better view of the evolution of pop1 and pop2 fluorescence emission during the synthesis (Figure 7a).

The emission maximum of pop1 shifts during the synthesis from 452 to 462 nm and from 490 to 512 nm for pop2 (Figure 7b, c). We interpret these red shifts as a decrease of the exciton confinement as the NPLs extend continuously laterally. At the onset of the NPL formation, the NPLs precursors have almost spherical shape (Figure 1a). The exciton is confined as in spherical NC. As the NPLs extend laterally, the exciton lateral confinement decreases, and the exciton emission red shifts. In the case of CdSe, the bulk exciton Bohr radius is r_{3D} = 5.6 nm. In the 2D limit of a quantum well, the exciton Bohr radius (r_{2D}) is 2 times smaller than the Bohr radius and increases with increasing well thickness.[28]

For NPLs with one lateral dimension < ~7 nm = $2r_{2D}$, the 2D exciton is laterally confined. The larger the lateral dimension is, the weaker the lateral confinement, and the lower the exciton energy. This explains the red shift of the emission wavelength with the maximum intensities during the NPLs lateral extension. For NPLs with lateral dimensions > ~7 nm, we expect that the electron and hole individual confinement is replaced by confinement of the exciton center of mass motion. The shift of the exciton lines in this case is inversely proportional to the very large hole effective mass and is much less sensitive to the lateral size of NPLs. This explains why the emission maximum does not shift anymore for the last three samples of Figure 7a that have lateral dimensions > 7 nm. The TEM data confirm this interpretation on the basis of spectroscopic arguments. Indeed, in Figure 1, we observed that the NPLs' smallest lateral dimensions grow from a few nanometers to about 20 nm as the maximum emission shifts from 450 nm to 462 nm. Similar observations were done with NPLs emitting at 510 nm (Figure S4 of the Supporting Information).

We have also analyzed emission spectra fwhm during the synthesis (Figure 7b, c). The fwhm of the two NPLs populations decreases almost steadily during the NPL growth (Figure 7b, c). It decreases from 12 to 7 nm for pop1 and from 22 to 9 nm for pop2. Such fwhm is very unusual and indicates that for pop1 and pop2, both the homogeneous and the inhomogeneous broadenings are much reduced compared to regular CdSe[29] NCs. As a comparison, in the case of the NCs (pop3), the fwhm increases steadily from 30 nm to 50 nm during the synthesis, which is characteristic of an increase in the size dispersion of the NCs. The decrease in the fwhm as the NPLs grow can be easily explained by modifications of the exciton lateral confinement. Indeed, when the NPLs lateral dimensions are small (~<7 nm), the exciton is laterally confined and inhomogeneity of the NPLs lateral dimensions results in different emission maximum and thus larger fwhm for ensemble measurements. On the contrary, for NPLs with lateral dimensions >7 nm, the 2D exciton is only weakly confined laterally, and variations in the lateral dimensions only weakly affect the emission maximum. This leads to minimum fwhm.

Nanoplatelets versus Magic Size Clusters. Magic-sized clusters have been considered as a possible explanation[30−32] for the absorption spectra presented in Figure 1h. The results we present in this work are in contradiction with this interpretation. The TEM images clearly show ultrathin homogeneous sheets. The argument that these sheets result from the aggregation of magic size clusters under the TEM[32] is hard to match with the folded NPLs observed in Figure 1d. Another argument in favor of the NPLs is the X-ray diffraction pattern which reveals very well resolved picks that would not be present in ensemble measurements

of small (<2 nm) clusters. Size-selective precipitation is yet another argument in favor of the NPLs. After NPLs synthesis, the reaction mixture often contains NPLs as well as nanocrystals. The NPLs can easily be separated from the other reaction products by addition of hexane and oleic acid (see Experimental Section) followed by a gentle precipitation at 5000 rpm The NPLs pellet down while the QDs remain in the supernatant. The last argument in favor of the NPLs is the red shift reported in Figure 1, in Figure 7, and in ref 31. As opposed to the continuous red shift that we observe, magic size clusters should have a well-defined shape and fixed emission and absorption spectra that evolve by steps as the cluster structure grows.

Synthesis of CdSe NPLs with Different Thicknesses. Slight variations of the protocols (see Experimental Section) used to synthesize 460 nm emitting NPLs give access to thicker NPLs emitting around 510 nm and 550 nm (Figure 8). All these NPLs have cubic crystal structures, and their growth mechanism can be followed as in the case of 460 nm NPLs with similar conclusions (Figure S4 of the Supporting Information). We observed slightly different values of the emission full width at half-maximum depending on the thickness of the NPL synthesized: 41 meV fwhm for the population emitting at 463 nm, 31 meV fwhm for the population emitting at 513 nm, and 35 meV for the one emitting at 550 nm. Such a small fwhm is to the best of our knowledge the smallest fwhm recorded so far at room temperature for semiconductor NCs in solution. The quantum yield of these NPLs can reach 50%, and the thicker the NPLs, the higher their quantum yields.

Interestingly, the emission spectra of each NPL population is best fitted with a Lorentzian rather than with a Gaussian (Figure 5). This suggests that the emission inhomogeneous broadening, leading to a Gaussian emission profile, is not dominant in these samples. At room temperature, the exciton line width results from several effects including phonon coupling,[33] spectral diffusion,[34] and photo-oxidation,[19] and it is unexpected that an fwhm so close to kT can be reached on ensemble measurements done in solution on $\sim 10^{12}$ NPLs simultaneously.

CONCLUSIONS

We have shown that the NPLs formation starts with ~2 nm diameter spherical NCs like particles that extend laterally to form NPLs with atomically controlled thickness. This extension has been analyzed using both TEM images and optical spectroscopy (fluorescence and absorption spectra) at different times during the NPLs synthesis for two kinds of syntheses that produce different NPL populations. The evolution of the NPLs fwhm and emission maxima during the syntheses is consistent with lateral extension of NC like particle into NPLs. It will be interesting to see whether NPLs structures can been extended to other type of semiconductors like CdS and CdTe.

ASSOCIATED CONTENT

Supporting Information. Four figures: two XRD patterns, one figure that describes the absorption spectra at constant volume of the CdSe NPLs population during lateral extension, and one figure that shows the growth stages of the NPLs emitting at 510 nm. This information is available free of charge via the Internet at http://pubs.acs.org.

AUTHOR INFORMATION

Corresponding Author
benoit.dubertret@espci.fr

ACKNOWLEDGMENT

We thank Mohamed Hanafi for precursor preparations and Al. Efros for many fruitful discussions and for critical reading of the manuscript. We thank the Agence Nationale de la Recherche, la Région Ile-de-France, and the Délégation Générale pour l'Armement. We thank X. Xu and P. Bassoul for help with the TEM maintenance and image acquisition. We thank N. Lequeux for valuable discussions and for help with the DRX measurements.

REFERENCES

(1) Jin, R. C.; Cao, Y. W.; Mirkin, C. A.; Kelly, K. L.; Schatz, G. C.; Zheng, J. G. *Science* **2001**, *294*, 1901–1903.
(2) Ah, C. S.; Yun, Y. J.; Park, H. J.; Kim, W. J.; Ha, D. H.; Yun, W. S. *Chem. Mater.* **2005**, *17*, 5558–5561.
(3) Puntes, V. F.; Zanchet, D.; Erdonmez, C. K.; Alivisatos, A. P. *J. Am. Chem. Soc.* **2002**, *124*, 12874–12880.
(4) Tian, Z. R. R.; Voigt, J. A.; Liu, J.; McKenzie, B.; McDermott, M. J.; Rodriguez, M. A.; Konishi, H.; Xu, H. F. *Nat. Mater.* **2003**, *2*, 821–826.
(5) Chang, Y.; Zeng, H. C. *Cryst. Growth Des.* **2004**, *4*, 397–402.
(6) Si, R.; Zhang, Y. W.; You, L. P.; Yan, C. H. *Angew. Chem., Int. Ed.* **2005**, *44*, 3256–3260.
(7) Cao, Y. C. *J. Am. Chem. Soc.* **2004**, *126*, 7456–7457.
(8) Sigman, M. B.; Ghezelbash, A.; Hanrath, T.; Saunders, A. E.; Lee, F.; Korgel, B. A. *J. Am. Chem. Soc.* **2003**, *125*, 16050–16057.
(9) Joo, J.; Son, J. S.; Kwon, S. G.; Yu, J. H.; Hyeon, T. *J. Am. Chem. Soc.* **2006**, *128*, 5632–5633.
(10) Schliehe, C.; Juarez, B. H.; Pelletier, M.; Jander, S.; Greshnykh, D.; Nagel, M.; Meyer, A.; Foerster, S.; Kornowski, A.; Klinke, C.; Weller, H. *Science* **2010**, *329*, 550–553.
(11) Yu, T.; Lim, B.; Xia, Y. N. *Angew. Chem., Int. Ed.* **2010**, *49*, 4484–4487.
(12) Tang, Z. Y.; Zhang, Z. L.; Wang, Y.; Glotzer, S. C.; Kotov, N. A. *Science* **2006**, *314*, 274–278.
(13) Son, J. S.; Wen, X. D.; Joo, J.; Chae, J.; Baek, S. I.; Park, K.; Kim, J. H.; An, K.; Yu, J. H.; Kwon, S. G.; Choi, S. H.; Wang, Z. W.; Kim, Y. W.; Kuk, Y.; Hoffmann, R.; Hyeon, T. *Angew. Chem., Int. Ed.* **2009**, *48*, 6861–6864.
(14) Murray, C. B.; Norris, D. J.; Bawendi, M. G. *J. Am. Chem. Soc.* **1993**, *115*, 8706–8715.
(15) Peng, X. G.; Manna, L.; Yang, W. D.; Wickham, J.; Scher, E.; Kadavanich, A.; Alivisatos, A. P. *Nature* **2000**, *404*, 59–61.
(16) Manna, L.; Milliron, D. J.; Meisel, A.; Scher, E. C.; Alivisatos, A. P. *Nat. Mater.* **2003**, *2*, 382–385.
(17) Ithurria, S.; Dubertret, B. *J. Am. Chem. Soc.* **2008**, *130*, 16504–16505.
(18) Ekimov, A. I.; Hache, F.; Schanneklein, M. C.; Ricard, D.; Flytzanis, C.; Kudryavtsev, I. A.; Yazeva, T. V.; Rodina, A. V.; Efros, A. L. *J. Opt. Soc. Am. B: Opt. Phys.* **1993**, *10*, 100–107.
(19) Wang, X. Y.; Qu, L. H.; Zhang, J. Y.; Peng, X. G.; Xiao, M. *Nano Lett.* **2003**, *3*, 1103–1106.
(20) Mahler, B.; Lequeux, N.; Dubertret, B. *J. Am. Chem. Soc.* **2010**, *132*, 953–959.
(21) Efros, A. L.; Rosen, M.; Kuno, M.; Nirmal, M.; Norris, D. J.; Bawendi, M. *Phys. Rev. B* **1996**, *54*, 4843–4856.
(22) Yu, W. W.; Qu, L. H.; Guo, W. Z.; Peng, X. G. *Chem. Mater.* **2003**, *15*, 2854–2860.
(23) Bowers, M. J.; McBride, J. R.; Rosenthal, S. J. *J. Am. Chem. Soc.* **2005**, *127*, 15378–15379.
(24) Kucur, E.; Ziegler, J.; Nann, T. *Small* **2008**, *4*, 883–887.
(25) Riehle, F. S.; Bienert, R.; Thomann, R.; Urban, G. A.; Krüger, M. *Nano Lett.* **2009**, *9*, 514–518.
(26) Kasuya, A.; Sivamohan, R.; Barnakov, Y. A.; Dmitruk, I. M.; Nirasawa, T.; Romanyuk, V. R.; Kumar, V.; Mamykin, S. V.; Tohji, K.; Jeyadevan, B.; Shinoda, K.; Kudo, T.; Terasaki, O.; Liu, Z.;

Belosludov, R. V.; Sundararajan, V.; Kawazoe, Y. *Nat. Mater.* **2004**, *3*, 99–102.

(27) Kudera, S.; Zanella, M.; Giannini, C.; Rizzo, A.; Li, Y. Q.; Gigli, G.; Cingolani, R.; Ciccarella, G.; Spahl, W.; Parak, W. J.; Manna, L. *Adv. Mater.* **2007**, *19*, 548–552.

(28) Bastard, G.; Mendez, E. E.; Chang, L. L.; Esaki, L. *Phys. Rev. B* **1982**, *26*, 1974–1979.

(29) Salvador, M. R.; Hines, M. A.; Scholes, G. D. *J. Chem. Phys.* **2003**, *118*, 9380–9388.

(30) Ouyang, J.; Zaman, M. B.; Yan, F. J.; Johnston, D.; Li, G.; Wu, X.; Leek, D.; Ratcliffe, C. I.; Ripmeester, J. A.; Yu, K. *J. Phys. Chem. C* **2008**, *112*, 13805–13811.

(31) Yu, K.; Ouyang, J.; Zaman, M. B.; Johnston, D.; Yan, F. J.; Li, G.; Ratcliffe, C. I.; Leek, D. M.; Wu, X. H.; Stupak, J.; Jakubek, Z.; Whitfiel, D. *J. Phys. Chem. C* **2009**, *113*, 3390–3401.

(32) Yu, K.; Hu, M. Z.; Waing, R. B.; Le Piolet, M.; Frotey, M.; Zaman, M. B.; Wu, X. H.; Leek, D. M.; Tao, Y.; Wilkinson, D.; Li, C. S. *J. Phys. Chem. C* **2010**, *114*, 3329–3339.

(33) Klein, M. C.; Hache, F.; Ricard, D.; Flytzanis, C. *Phys. Rev. B* **1990**, *42*, 11123–11132.

(34) Neuhauser, R. G.; Shimizu, K. T.; Woo, W. K.; Empedocles, S. A.; Bawendi, M. G. *Phys. Rev. Lett.* **2000**, *85*, 3301–3304.